

Spin transport and temperature-dependent giant positive junction magnetoresistance in $\text{CoFe}_2\text{O}_4/\text{SiO}_2/p\text{-Si}$ heterostructure

J. Panda¹ · T. K. Nath¹

Received: 12 June 2015 / Accepted: 4 December 2015 / Published online: 11 January 2016
© Springer-Verlag Berlin Heidelberg 2016

Abstract The observation of giant positive junction magnetoresistance (JMR) in our cobalt ferrite (CFO)/p-Si heterojunction has been reported here. The pulsed laser deposition technique has been used for fabrication of the heterojunction. The junction confirms a very good rectifying magnetic diode like behavior at low temperature, whereas at high temperatures the junction shows nonlinear I - V characteristics. The magnetic field-dependent magnetoresistance (MR) of both CFO film and across the heterojunction have been studied in detail. The CFO film shows negative MR behavior, whereas the junction shows large positive JMR behavior throughout the temperature range. The spin lifetime (142 ps) and spin diffusion length (331 nm) have been estimated of the heterostructure at 10 K. The highest JMR value ($\sim 1600\%$) has been observed at 10 K, and it gradually decreases at higher temperature range. The origin of positive JMR in our heterojunction has been best explained by the standard spin injection theory.

1 Introduction

Spin electronics exploits the spin of the electron, rather than its charge, for information storage and processing [1–3]. One of the main possibilities of spin transport electronics or spintronics is efficient spin injection into a semiconductor (SC) medium from a highly spin-polarized source and successful manipulation and detection of the

injected spin-polarized electrons in multifunctional and novel spintronic devices [1]. There are several reports, both theoretical [4] and experimental [5], on spin injection from spin-polarized ferromagnetic metal to SCs through insulating tunnel barriers in a ferromagnet (FM)/SC heterostructure found in the literature. The intense attention in silicon spintronics rises from the expected long spin coherence length and its industrial dominance [6]. Injection of spin-polarized carriers in Si by using polarized light [7], hot electrons spin injection [8], tunnel spin injection [9–17], Seebeck spin tunneling [18], and dynamical spin pumping methods have been observed recently [19]. The injection of spin-polarized electron using ferromagnetic tunnel contacts to inject and detect spin polarizations in Si has been identified as the most possible and robust method among them [8, 20]. Several groups have explained well about the spin injection and spin transport in Si [8, 10, 13, 21, 22], and most of the work has focused on using an insulating tunnel oxide layer such as Al_2O_3 or MgO with a FM metal as a spin injecting contact. There are number of reports where the native SiO_2 oxide layer is extensively used in the electronics industry and serves as an excellent spin tunnel barrier in FM/ SiO_2 /Si structures [14]. The tunnel barrier is used to overcome the large difference in conductivity between metal and the semiconductor that would otherwise make spin injection impossible [4, 23]. Apart from ferromagnetic materials, other materials having high Curie temperature and large spin polarization, like spinel ferrites, can be considered as potential candidates for ferromagnetic electrodes in FM/SC heterostructure. Three of the most widely studied spinel ferrites are magnetite (Fe_3O_4), cobalt ferrite (CoFe_2O_4), and nickel ferrite (NiFe_2O_4). Among these ferrites, Fe_3O_4 is a half-metal (100 % spin polarization) having conduction through hopping of down spins among B-sites in the spinel

✉ T. K. Nath
tapnath@gmail.com; tnath@phy.iitkgp.ernet.in

¹ Department of Physics, Indian Institute of Technology Kharagpur, Kharagpur, West Bengal 721302, India

structure [24–26]. Spinel ferrites CoFe_2O_4 and NiFe_2O_4 are not half-metal, rather semi-insulator magnetic oxides with high magnetic ordering temperatures and large saturation magnetizations [27]. This rare combination of properties makes them very attractive for a wide range of applications. CoFe_2O_4 and NiFe_2O_4 can effectively be used as spin filters in heterostructure devices [28, 29]. Among various ferrite materials, a spinel-type CoFe_2O_4 (CFO) is a well-known hard magnetic material which has been studied in detail exhibiting high coercivity, moderate saturation magnetization, remarkable chemical stability, and mechanical hardness [30, 31] as well as largest magnetostriction in the spinel ferrites. Growths of thin cobalt ferrite films have been reported in the past by various methods; the most used being pulsed laser deposition (PLD) from a CoFe_2O_4 target. There are a few reports on the CFO thin film, which was deposited on MgO [32], SrTiO_3 , MgAl_2O_4 [33–35], and Si [36] substrates in order to study the structural properties of CFO film. However, mass-produced spin electronics devices require inexpensive substrates. Silicon substrates fulfill these conditions and, furthermore, have a good flatness. Electrical properties of films deposited on silicon substrates covered with an ultrathin native oxide layer have been seen to behave differently than films on bare silicon or thermally oxidized silicon substrates. In the presence of interface states, the Fermi level may be pinned at the Si-SiO_2 interface, leading to band bending and the formation of depletion layer [37]. In addition to the structural properties of CFO thin film, a thorough understanding of the electronic and magneto-transport properties of both the film and across the junction is essential before attempting to synthesize better spintronics devices with these materials.

In this work, we report the fabrication of CFO (semi-insulating, $T_C = 858$ K) magnetic thin film/p-Si non-magnetic semiconductor heterojunction and study the detail electronic transport properties of our heterojunction. We have explicitly studied in detail the junction current–voltage (I – V) characteristics of the heterojunction without and with external magnetic field up to 6 T in the temperature range of 10–300 K. The magnetic field-dependent magnetoresistance behavior of the CFO film (top film) and the same heterojunction have also been studied in the same temperature range. The heterojunction shows a very good rectifying magnetic diode like behavior at low temperature, and at higher temperatures, the junction shows nonlinear I – V behavior. The CFO film shows negative magnetoresistance behavior, whereas the junction shows positive junction magnetoresistance (JMR) behavior throughout the temperature range. The highest positive JMR (~ 1600 %) has been observed at 10 K, and the magnitude of positive JMR value decreases at high temperatures. The origin of positive JMR in our

heterojunction has been best explained by the standard spin injection theory.

2 Experimental details

2.1 Device fabrication

The single-phase CoFe_2O_4 powder have been prepared by taking required amount of high-purity Co_3O_4 and Fe_2O_3 powders, mixed well with hand grinder repeatedly and sintered at 900 °C. Finally, the CFO powder was pelletized and used as the target for pulsed laser deposition. The p-Si (001) substrate was well cleaned to remove organic and inorganic compounds and finally etched for 5 min using hydrofluoric acid preceding to loading into the high vacuum thin film pulsed laser deposition chamber. The carrier concentration (n) and resistivity (ρ) of the p-Si (001) substrates were determined at room temperature using Hall effect measurement system (Ecopia, South Korea, HMS 5300), and it is found to be $n = 4 \times 10^{16} \text{ cm}^{-3}$ and $\rho = 3 \text{ } \Omega\text{-cm}$. The CFO film (125 nm) was deposited on well-cleaned p-Si (100) substrate in 0.5-mbar O_2 partial pressure (base pressure $\sim 2 \times 10^{-6}$ Torr). The substrate temperature was kept at 650 °C during the growth process of CFO film. The repetition rate of the laser pulse was kept at 10 Hz, and the fluence at the target surface was 2 J/cm^2 . The distance between the substrate and target was 5 cm in the chamber. After deposition, the film was sintered at the same physical condition for 1 h to get well-crystalline samples.

2.2 Device characterization and measurement setup

The high-resolution X-ray diffraction (HRXRD, Philips pan analytical x-pert) with Cu-K_α radiation ($\lambda \sim 1.542 \text{ } \text{Å}$) has been used for structural characterization of our heterostructure. The chemical composition of the as-grown thin film has been determined using X-ray photoelectron spectroscopy (XPS, PHI 5000 Versa Probe II Scanning). The quality of interfacial properties of the heterojunction was characterized by cross-sectional high-resolution transmission electron microscopy (JEM—2100 HRTEM, JEOL, Japan). The operating voltage was used $\sim 200 \text{ keV}$ in the high-resolution transmission electron microscope. The surface morphology and rms surface roughness of as-grown film have been recorded using an atomic force microscope (AFM Model: 5500, Make: Agilent) in tapping mode. The temperature-dependent electronic and magneto-transport properties of the heterojunction have been investigated in detail employing a cryogen-free high magnetic field up to 8 T and low-temperature (down to 1.6 K) (superconducting magnet) VTI cryostat system

(CFM VTI 8 T, Cryogenics, UK) in the temperature range of 10–300 K, a source-measure unit (SMU, Keithley-2612) with 1 μV resolution, and a 7 $\frac{1}{2}$ -digit Digital Multi-Meter (Keithley-2000) along with a high-precision temperature controller (Lakeshore-340, USA). The magnetic properties of the CFO film were measured using a superconducting quantum interference device (SQUID, Quantum design) DC magnetometer at different isothermal conditions. For electronic transport properties, good ohmic contacts have been made by using ‘In’ metal contacts on both CFO thin film and p-Si substrate.

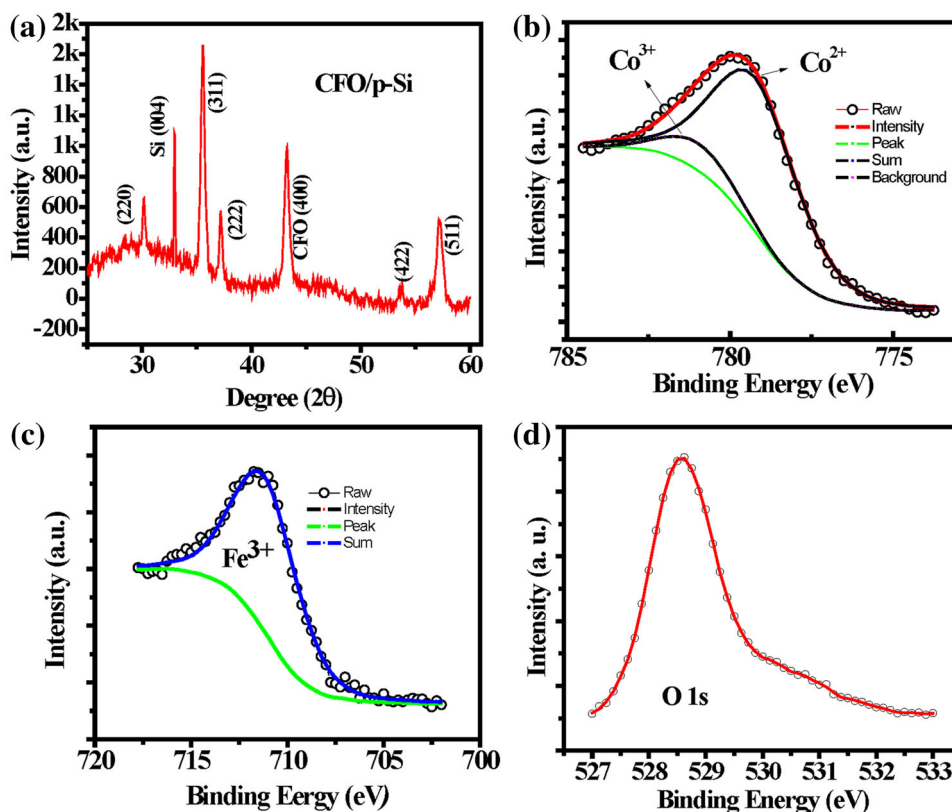
3 Results and discussion

3.1 Structural studies

The XRD pattern of the polycrystalline CFO/p-Si heterojunction is shown in Fig. 1a. In Fig. 1a, all the diffraction peaks (220), (311), (222), (400), (422), and (511) are from CFO film only. No other secondary phase was observed. All the diffraction peaks of the CFO film are observed with different orientation on the p-Si (100) substrate. The overall chemical composition of cobalt ferrite film was obtained from the XPS analysis. In the XPS analysis, the

samples are generally exposed to the monochromatic X-ray radiation. Figure 1b–d present the XPS spectra of synthesized cobalt ferrite film showing peaks for Co 2p, Fe 2p, and O 1s core levels, respectively. The film was composed of Co, Fe, and O with corresponding binding energies of 779.1 (Co 2p_{3/2}), 711.6 (Fe 2p_{3/2}), and 529.3 eV (O 1s), respectively. The Co 2p_{3/2} XPS spectra are fitted well into two peaks situated at 779.6 and 781.3 eV. The binding energies at 779.6 and 781.3 eV are assigned to Co²⁺ and Co³⁺. The presence of a large number of Co²⁺ species in our CFO film can be confirmed by the intense Co2p_{3/2} peak, due to the fact that the low-spin Co³⁺ cation only provides weaker peak than high-spin Co²⁺ with unpaired valence 3d electron orbitals. In Fe 2p_{3/2} main peak, the fitted signals positioned at 711.6 eV, indicating the existence Fe³⁺ ions in octahedral sites. The analysis of the Co 2p, Fe 2p, and O 1s peaks offered Co:Fe and Fe:O atomic ratios close to 1:2 and 1:2, respectively, as expected for the stoichiometric composition of cobalt ferrite. These values match very well to the reported values in the literature [38]. The XPS results were consistent to HRXRD observations, confirming the formation of single-phase cobalt ferrite rather than mixed phases of CoO and Fe₂O₃. These observations clearly suggest that the single-phase cobalt ferrite thin film has been grown on p-Si (001) substrate.

Fig. 1 a The XRD pattern of CFO/p-Si heterojunction. b, c, d The XPS spectra of synthesized cobalt ferrite film for Co 2p, Fe 2p, and O 1s core levels, respectively



3.2 Electrical transport properties of the heterojunction

The electronic transport properties across the junction have been investigated in the temperature range of 10–300 K. We have recorded current–voltage (I – V) characteristics of the CFO/p-Si heterojunction interface without and with 6 T applied magnetic field at various temperatures as shown in Fig. 2a, b, respectively. From the recorded I – V characteristics, the current across the junction with applied DC voltage through the interface shows nonlinear behavior at high temperatures (above 150 K), whereas a strong nonlinearity and good rectifying behavior have been observed at low temperatures (below 150 K). The I – V curves in the low-temperature regime clearly show asymmetric nature with excellent rectifying magnetic diode like behavior without and with applied 6 T magnetic field. The contacts between In/CFO and p-Si/In show very good ohmic

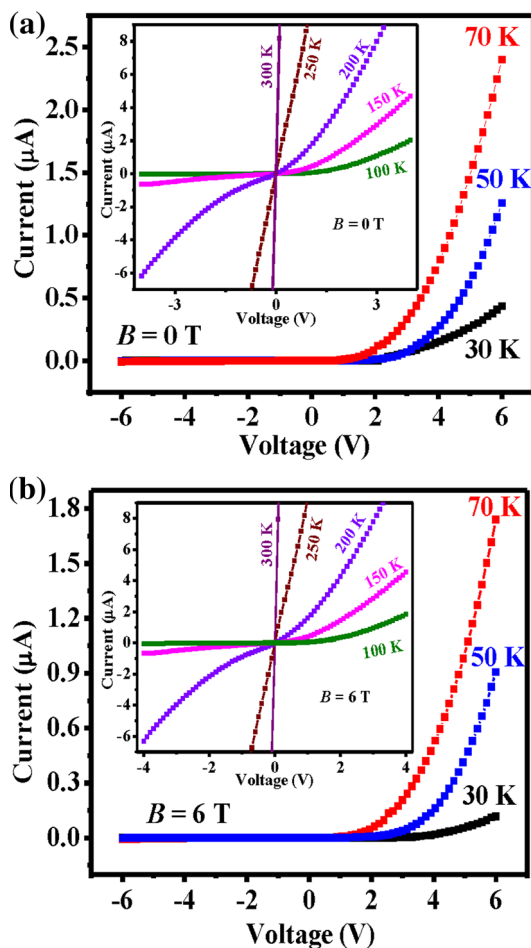


Fig. 2 a, b The I – V characteristics of the heterojunction at different isothermal conditions in the temperature range of 10–300 K without and with applied 6 T magnetic field

behavior (not shown here). The contact resistance was found to be less than 2Ω . Therefore, it can be clearly confirmed that the nonlinear I – V curves are observed from the junction (CFO/SiO₂/p-Si) only, not due to the metal contacts on CFO and p-Si. The junction resistance includes CFO magnetic thin film, SiO₂ native oxide and p-Si substrate. The polarity is such that the forward bias corresponds to the application of a positive DC bias voltage to the p-Si substrate. According to the theory of thermionic emission [39], the junction I – V characteristics can be described as,

$$I = I_0 \exp\left(\frac{e(V - IR_s)}{\eta k_B T}\right) \quad (1)$$

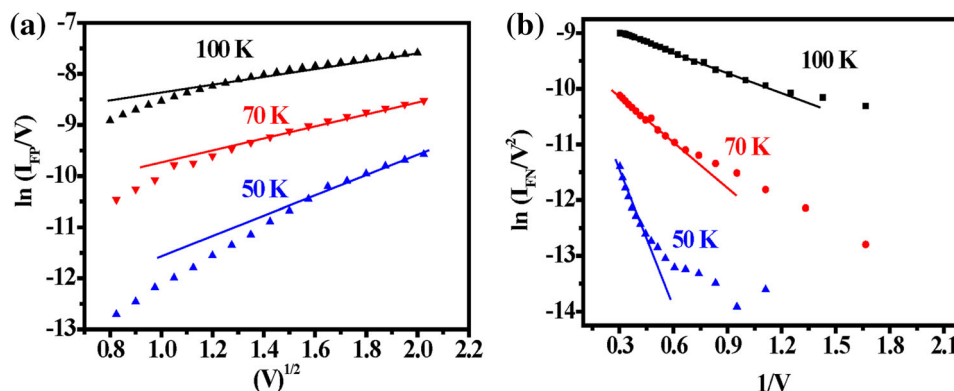
where T , k_B , η , e , R_s , and I_0 represent the temperature, Boltzmann constant, ideality factor, elementary electronic charge, junction series resistance, and reverse saturation current, respectively. From the data, the ideality factor η and the reverse saturation current $I_0 = AA^*T^2 \exp\left(\frac{e\phi_B}{k_B T}\right)$

were extracted (not shown here), where $A^* = \frac{em^*k_B^2}{2\pi^2\hbar^3}$ denotes the Richardson constant, e the electronic charge, m^* the effective mass, \hbar the Planck's constant divided by 2π , k_B the Boltzmann constant, ϕ_B the Schottky barrier height, and A the active junction area. The ideality factor is much greater than 2 at all temperatures, indicating that the I – V curves might be because of some tunneling transport mediated by pinholes in the barrier [23, 40, 41]. Hence, it is necessary to find out the possible tunneling mechanism across the heterojunction. The observed field-stimulated emission and capture have been discussed in terms of Fowler–Nordheim (F–N) tunneling [42], the Poole–Frenkel effect [43–45], phonon-assisted tunneling [46], and a combination of both phenomena [44]. F–N tunneling is the process whereby electrons tunnel through a barrier in the presence of a high electric field. This quantum-mechanical tunneling process is an important mechanism for thin barriers as those in metal–semiconductor junctions on highly doped semiconductors. F–N tunneling current through a triangular barrier at high electric field is given by [42]

$$J_{FN} = AV^2 \exp(-B/V), \quad (2)$$

where $A = q^3/8\pi\hbar\phi_B$ and $B = 8\pi(2m_{FN})^{1/2} \phi_B^3/3qh$. Here q is the electronic charge and ϕ_B and m_{FN} are the effective tunneling barrier height and effective mass of electron for F–N tunneling. V is the applied voltage. The high-field F–N tunneling should be temperature independent. But our observed $(\ln(I_{FN}/V^2))$ versus $1/V$ is strongly temperature-dependent at this field range (Fig. 3b), and hence, we can conclude that the field-dependent tunneling is mainly temperature-dependent Frenkel–Poole-type emission.

Fig. 3 **a** Poole–Frenkel plots of CFO/p-Si heterojunction in the absence of magnetic field. **b** F–N plots for the same heterojunction at 0 T field



The well-known Poole–Frenkel effect describes the increase in the thermal emission rate of carriers in an external electric field due to the lowering of the barrier associated with their Coulomb potential. It is a classical mechanism in which the electron is thermally emitted over the top of a potential barrier which has been lowered by the presence of an electric field. The Poole–Frenkel emission refers to the electric-field-enhanced thermal emission from a trap state into a band of electronic states of insulator's conduction band. The current density associated with the Poole–Frenkel emission is given by [47]

$$I_{FP} = CV \exp \left[-\frac{q \left(\phi_B - \sqrt{\frac{qV}{\pi \epsilon_0 \epsilon_s}} \right)}{k_B T} \right] \quad (3)$$

where ϕ_B is the barrier height for electron emission from the trap state and ϵ_s is the relative dielectric permittivity at high frequency, rather than the static dielectric constant [43]. The electrons in the electrode are able to transit to the bound states originating from the traps in the insulator at the metal/insulator junction by quantum–mechanical tunneling. The transition of electrons from the electrode to the conduction band of the insulator via the traps is generally defined as the tunneling-assisted Poole–Frenkel conduction [48].

The high-field $\ln(I_{FP}/V)$ versus \sqrt{V} plots at $H = 0$ shown in Fig. 3a are almost linear at high electric field for all temperatures, and it strongly implies that the temperature-dependent tunneling-assisted Poole–Frenkel emission is the dominating current transport mechanism in CFO/p-Si heterojunction across the narrow intermediate native oxide SiO₂ layer. The strongly temperature-dependent tunneling-assisted Poole–Frenkel emission mainly originates from activated emission at the CFO/p-Si interface barrier of this FM/SC spintronic device heterostructure.

Figure 4a shows the $\ln(I_0/T^2)$ versus $1/T$ plot of the CFO/p-Si heterojunction. The barrier height (ϕ_B) of CFO/p-Si was estimated to be 0.74 eV according to the equation,

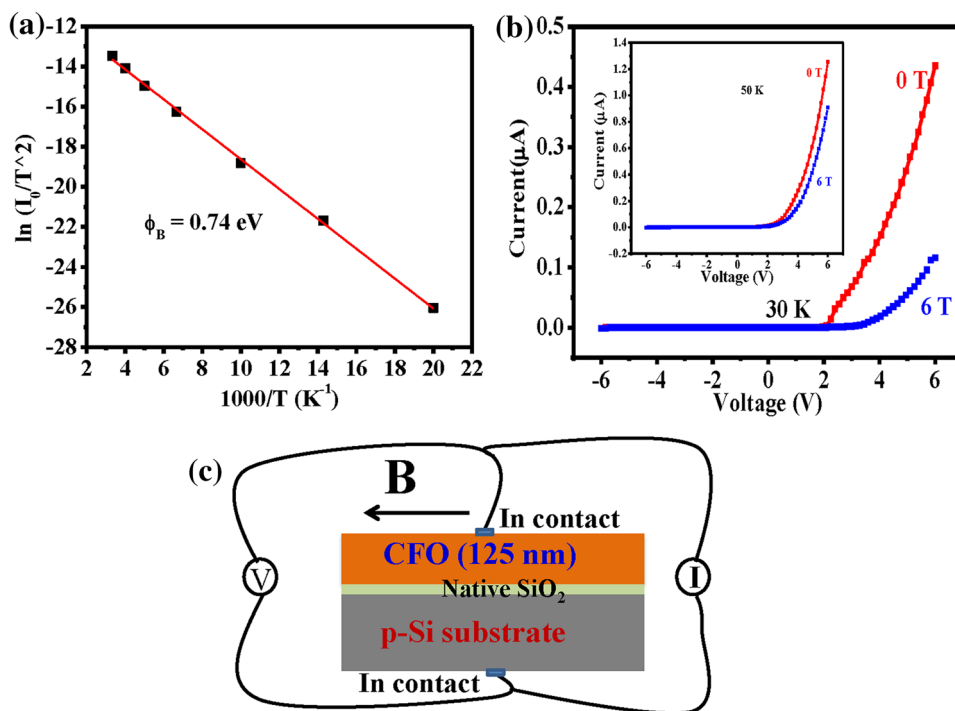
$$\ln \left(\frac{1}{T^2} \right) = \ln(A_e A^*) - \frac{q(\phi_B - V)}{k_B T} \quad (4)$$

The comparative study of I – V characteristics for CFO/p-Si heterojunction without and with applied 6 T magnetic field have been carried out at different isothermal conditions. Figure 4b shows the comparative I – V characteristics at 30 K, and the inset shows at 50 K. From Fig. 4b, we can conclude that the junction current is noticeably reduced by the application of applied magnetic field in forward bias, and there was no change in the junction current in reverse bias (negligible). Therefore, the junction resistance (CFO/SiO₂/p-Si) increases by the applied 6 T magnetic field exhibiting positive junction magnetoresistance (JMR) behavior of CFO/p-Si heterojunction. The schematic diagram of our heterojunction has been shown in Fig. 4c. To investigate the electronic transport properties of the heterojunction, the DC bias voltage has been applied across the junction and the junction current across the interface has been recorded. The external magnetic field (6 T) has also been applied parallel to the direction of the film plane in order to study the effect of magnetic field on junction current in our heterojunction. The highly conducting high-purity In metal contacts were made for ohmic contact on both CFO film and p-Si substrate.

3.3 Junction magnetoresistance properties of the heterojunction

The magnetoresistance properties of both CFO film and the junction have been investigated at a constant temperature. The magnetic field-dependent MR properties of the CFO film have been investigated at different isothermal conditions for a constant current of 0.1 mA in the in-plane (CIP) direction in the temperature range of 100–300 K. A separate CFO thin film has been deposited on α -Al₂O₃ (0001) sapphire insulating substrate (CFO/ α -Al₂O₃) under the same physical conditions using pulsed laser deposition

Fig. 4 **a** The $\ln(I/T^2)$ versus I/T plot for the heterojunction at zero magnetic field to obtained barrier height using Eq. 4. **b** The comparative $I-V$ study without and with applied 6 T magnetic field at 30 and 50 K (inset of Fig. 3b). **c** The schematic diagram of the heterojunction where the DC bias voltage applied across the junction and the external magnetic field was applied parallel to the film plane



technique in order to prevent conduction through the p-Si substrate in the CFO/p-Si heterostructure. For electrical transport measurements, the four probe contacts were made on the CFO film with ‘In’ ohmic contact. We can safely assume that all the current flows through the CFO film plane only in CFO/ α -Al₂O₃ heterostructure. The change of resistance with applied magnetic field parallel to the film plane up to a magnetic field of 6 T has been recorded for CFO magnetic thin film for current in-plane direction (CIP geometry). We calculate the magnetoresistance of the CFO film directly from the recorded resistance data using the standard formula,

$$\%MR = \frac{R_H - R_0}{R_0} \times 100 \tag{5}$$

where R_H and R_0 are the resistance with and without applied magnetic field, respectively. The magnetic field-dependent JMR properties of the CFO/SiO₂/p-Si heterojunction have been observed at different isothermal conditions for fixed forward DC bias voltage of 4 V. The change in current with applied magnetic field parallel to the film plane up to 6 T has been observed across the junction (CFO/SiO₂/p-Si) for current perpendicular to the plane direction (CPP geometry). The reverse bias current being negligible (<0.1 μ A, excellent rectifying behavior) in the device, the change in the current with the application of magnetic field could not be measured due to the limitation

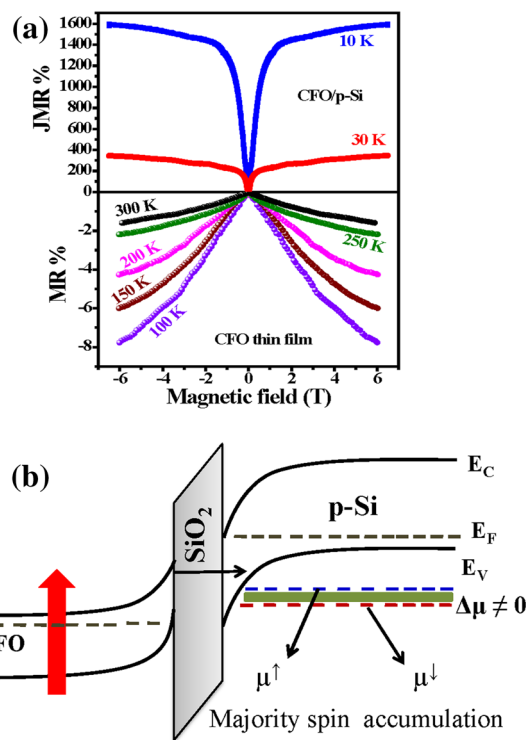


Fig. 5 **a** The MR behavior of both CFO magnetic thin film and the junction at different isothermal conditions. **b** The schematic energy band profile of the heterojunction and spin injection, spin accumulation in valence band of p-Si

of the measuring instruments. Figure 5a shows the MR behavior of both CFO film and the junction. The magnetic thin film (CFO) shows negative MR, whereas the junction shows positive JMR behavior throughout the working temperature range. Highest negative MR% of CFO film (top layer) has been observed to be $\sim 8\%$ at 100 K at a magnetic field of 6 T and gradually decrease with increasing temperature. The magnetoresistance of the p-Si (001) substrate is negligible throughout the temperature. So we can clearly confirm that the origin of observed JMR mainly from the junction only—not due to the individual properties of either CFO magnetic thin film or p-Si non-magnetic semiconductor. The value of %JMR across the junction has been calculated using Eq. (5). The value of positive JMR has been observed to be 1600 and 370 % at a biasing voltage of 4 V at 10 and 30 K, respectively. The origin of the JMR in this heterostructure can be explained by the standard electrical injection of a spin-polarized tunnel current. There are several reports in the literature to prove the spin accumulation in nonmagnetic Si substrate using 3-terminal Hanle curve experiment [2, 5, 49, 50]. We have not shown here the accumulated spin signal in p-Si substrate using 3-terminal Hanle curve. When the spin-polarized electrons are injected from the half-metallic ferromagnetic material to semiconductor (SC), it produces majority spin accumulation in conduction band of the SC; when the spin-polarized electrons are extracted from the SC to half-metallic ferromagnetic material, it produces minority spin accumulation in conduction band of SC. As a result, the spin accumulation produces an imbalance in the electron population in the Si conduction band or in the hole population in the valence band (see Fig. 5b for p-type Si) [3, 4, 23]. This is described by different electrochemical potentials, μ^\uparrow and μ^\downarrow , for the up and down spins, respectively, and a spin accumulation is defined as $\Delta\mu = \mu^\uparrow - \mu^\downarrow$. Based on the spin injection theory, when the spin-polarized electrons or holes are injected from ferromagnetic material to semiconductor, it produces majority spin accumulation in conduction band or valence band of the SC. As a result, the spin accumulation produces an imbalance in the electron population in the Si conduction band or in the hole population in the valence band (see the proposed diagram in Fig. 5b for p-type Si). The direction of the spin polarization is determined by the magnetization direction of the magnetic thin film, and it is parallel to the interface (that is, in-plane). The spin accumulation in nonmagnetic semiconductor is greatest directly underneath the contact and decays with increasing distance from the interface with certain spin diffusion length (L_{SD}). In the present case, the spin-polarized holes creates nonequilibrium spin population (majority hole spin accumulation) in valence band of p-type Si. In forward bias, the spin-polarized holes from

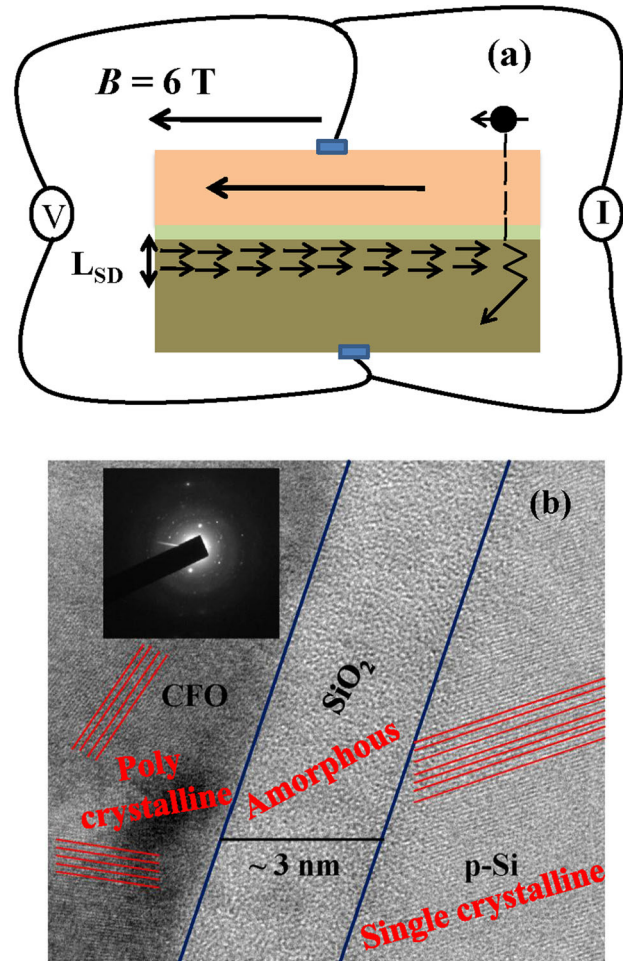


Fig. 6 **a** The schematic diagram of the proposed model of the CFO/p-Si heterostructure where the spin-polarized carriers moving across the interface will undergo large spin-dependent scattering in the presence of saturation external magnetic field within the L_{SD} . **b** The cross-sectional HRTEM of the CFO/SiO₂/p-Si heterostructure and inset shows the SAED pattern of the CFO thin film

the CFO magnetic thin film tunnel through the SiO₂ layer and accumulate in valence band of p-Si. These accumulated spins create nonequilibrium population in net spin density of states in valence band at fermi level in p-type Si within L_{SD} . Figure 5b shows the proposed schematic diagram of the CFO/p-Si heterostructure where the maximum spin accumulation is observed in p-Si in the absence of external magnetic field within the spin diffusion length. When we apply a saturation magnetic field parallel to the film plane, the magnetization of the magnetic film attains its saturation value via domain orientation in the direction of the applied magnetic field. The bottom layer is expected to be aligned in an antiparallel orientation to the top magnetic film, similar to the case of a magnetic tunnel junction (MTJ) [51–53]. The magnetic moments of the CFO layer (top layer on oxide) and the spin accumulation

layer near the valence band in semiconductor (bottom layer below oxide) are alternately coupled in antiparallel (oscillating behavior) direction via insulating tunnel barrier through the RKKY-type indirect exchange interaction as shown in Fig. 6a. Similar to the GMR/TMR device, the spin-polarized carriers moving across the interface will undergo large spin-dependent scattering from the induced magnetic spin accumulation region (within L_{SD}), thus producing a high resistive condition of the device under application of the external magnetic field. Therefore, the resistance across the junction increases with applied magnetic field and we observe positive JMR in our heterojunction.

Figure 6b shows the cross-sectional HRTEM image of the CFO/SiO₂/p-Si heterojunction. The HRTEM image clearly reveals the growth of polycrystalline CFO film (125 nm) on the p-Si substrate, and the film was well separated from the p-Si substrate through a native SiO₂ layer (~3 nm) with sharp interfaces. The polycrystalline nature of the film was also established from the selected area electron diffraction patterns (inset of Fig. 6b) which also showed the absence of any secondary phases. A close look at the interface reveals the existence of a layer of thickness 3–4 nm between ferrite film and p-Si substrate, and this is expected to be thin native SiO₂ layer. The presence of this insulating interfacial layer must play an important role in the observed transport properties of the heterostructures.

Figure 7a shows the temperature-dependent JMR% of the heterojunction at 6 T magnetic field in the temperature range of 10–300 K. The noticeably high value of positive JMR has been observed at 10 K (~1600%). The magnitude of JMR gradually decreases at higher temperature regime. At higher temperature, the frozen carriers in the semiconductor attain thermal energies through phonon vibrations which dominate over the magnetic energy responsible for the formation of hole spin accumulation in the silicon. The surface morphology of the as-grown magnetite thin film has been recorded using tapping mode AFM. The 2-D AFM image of the as-grown magnetite thin film in the scan area of (1.5 μm × 1.5 μm) has been shown in inset of Fig. 7a. The surface morphology clearly shows that the film is uniformly grown on the surface of the single-crystalline (001) p-Si substrate with full coverage. The average rms surface roughness of the film has been found to be 0.7–0.9 nm. Figure 7b shows the change in spin-polarized tunneling current with the applied magnetic field in the silicon at 10 K for a constant applied bias voltage of 4 V across the CFO/p-Si heterojunction. From Fig. 7b, it can be observed that the spin-polarized junction current gradually decreases with applied magnetic field within L_{SD} in valence band of p-Si semiconductor. The spin-polarized carriers moving across the interface will

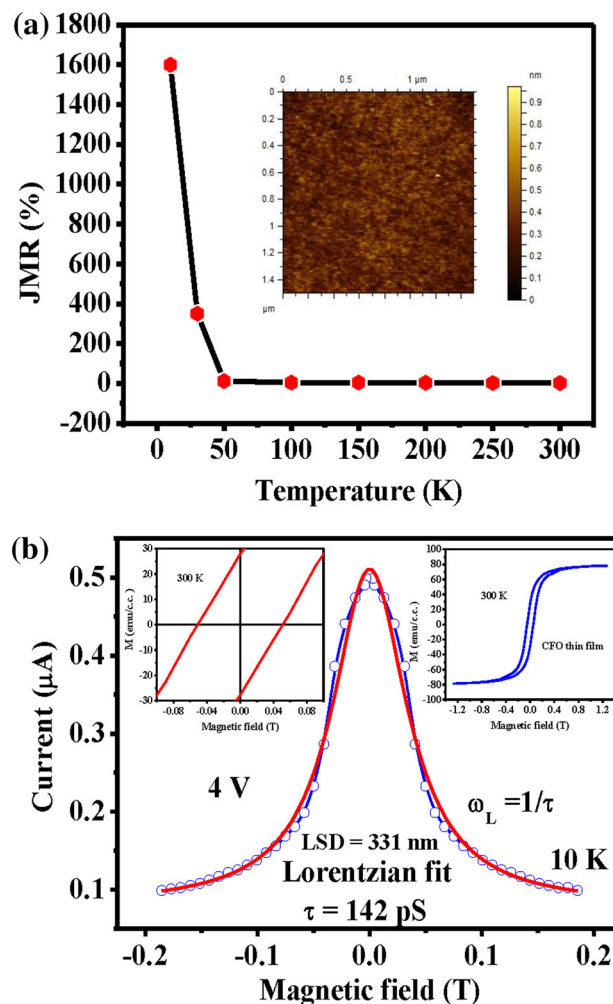


Fig. 7 **a** The magnetic field-dependent junction current of the CFO/p-Si heterojunction at different isothermal conditions (10 and 30 K) and inset shows the 3D AFM image of the surface morphology of the CFO thin film. **b** The change in spin-polarized tunneling current with the applied magnetic field in the silicon at 10 K for a constant applied bias voltage of 4 V across the CFO/SiO₂/p-Si heterojunction, and *right inset* shows the $M(H)$ behavior of the CFO film at 300 K. *Left inset* shows magnified view of the same $M(H)$ plot in the low-field regime

undergo large spin-dependent scattering from the spin accumulation region (L_{SD}), thereby producing a high resistive condition (positive JMR) of the device under application of the external magnetic field parallel to the in-plane direction of the magnetic thin film. The forward bias junction current decays as a function of magnetic field B with an approximately Lorentzian line shape. With certain order of approximation [9], it could be easily derived that the current across such a device in the presence of a magnetic field (B) can be written as [54] $I(B) = \frac{I(0)}{(1+(\omega_L \tau)^2)}$, where τ is the spin lifetime and the Larmor frequency, $\omega_L = \frac{g\mu_B B}{\hbar}$, where g is the Landé g -factor, μ_B is the Bohr

magneton, and \hbar is Planck's constant divided by 2π . The signal is described reasonably well by a Lorentzian line shape (red line shape). From the full width at half maximum (FWHM) of the curve (Fig. 7b) taking $g = 2$, we obtain the spin lifetime $\tau = 142 \text{ ps} \pm 2 \text{ ps}$. We have also calculated spin diffusion length (L_{SD}), $L = \sqrt{D\tau}$ in the Si, where D is the diffusion coefficient ($7.7 \text{ cm}^2/\text{s}$) derived from the electron mobility ($9000 \text{ cm}^2/\text{Vs}$) using temperature-dependent Hall measurement system at 10 K for p-Si with a doping concentration of $4 \times 10^{16} \text{ cm}^{-3}$. With $\tau = 142 \text{ ps}$, we get $L_{SD} = 331 \text{ nm}$ at 10 K for our p-type Si in the heterostructure. The right inset of Fig. 7b shows the magnetic properties of the CFO thin film at room temperature. From magnetization measurements $M(H)$, we confirm that the CFO thin film show ferrimagnetic hysteresis behavior at 300 K. The CFO film saturates at low field. The left inset of Fig. 7b shows the magnified view of the same $M(H)$ plot in the low-field regime showing coercive field value $H_c = 500 \text{ Oe}$. Though the CFO film shows ferrimagnetic behavior even at room temperature, the JMR of the heterojunction is not significant at room temperature. It falls sharply and becomes insignificant beyond 50 K (Fig. 7a). Therefore, the JMR of the heterojunction depends on spin polarization of the CFO film, CFO/SiO₂/p-Si interface, and the intrinsic properties (viz. doping concentration and carrier mobility) of the semiconductor.

4 Conclusions

In summary, we have grown successfully the single-phase CFO magnetic thin film on p-Si substrate using pulsed laser deposition technique. From electronic transport study, I - V characteristics of the heterojunction show a very good rectifying magnetic diode like behavior at low temperature, and at higher temperatures, the junction shows nonlinear I - V behavior. The magnetic field-dependent magnetoresistance behavior of the CFO and the same heterojunction has been studied at different isothermal conditions. The CFO film shows negative magnetoresistance behavior, whereas the junction shows positive JMR behavior throughout the temperature range. The spin lifetime (142 ps) and spin diffusion length (331 nm) have been estimated for our heterostructure at 10 K. The origin of JMR in the device has been explained using spin injection theory in the semiconductor where the electrical spin injection of hole from the CFO film into the Si substrate takes place, producing an imbalance of majority hole spin accumulation in the valence band of p-Si. The highest positive JMR ($\sim 1600\%$) has been observed at 10 K. The magnitude of JMR value decreases with increasing temperature. At higher temperature, the

frozen carriers in the semiconductor acquire thermal energies through phonon vibrations which dominate over the magnetic energy responsible for the formation of electron spin accumulation in the silicon. The JMR of our heterostructure saturates at a much lower magnetic field as compared to the other earlier reported heterostructures. Therefore, this high value of JMR in our heterostructures can be used as promising spin diode like unit (component) and normal GMR/TMR like devices, extremely useful for spintronics applications.

Acknowledgments Authors would like to acknowledge the help of Dr. D. M. Phase and Dr. Ram Janay Choudhary (UGC DAE, Indore) during growth of heterostructure. One of the authors (TKN) would like to acknowledge the financial assistance of IIT Kharagpur through SGIRG challenge grant project with Project Code IIT/SRIC/PHY/UBF/2014-15/137.

References

1. I. Žutić, J. Fabian, S.D. Sarma, Rev. Mod. Phys. **76**, 323 (2004)
2. C. Chappert, A. Fert, F.N. Van Dau, Nat. Mater. **6**, 813 (2007)
3. D. Awschalom, M. Flatte, Nat. Phys. **3**, 153 (2007)
4. E.I. Rashba, Phys. Rev. B **62**, R16267 (2000)
5. S.P. Dash, S. Sharma, R.S. Patel, M.P. Jong, R. Jansen, Nature (London) **462**, 491 (2009)
6. R. Jansen, S.P. Dash, S. Sharma, B.C. Min, Semicond. Sci. Technol. **27**, 083001 (2012)
7. G. Lampel, Phys. Rev. Lett. **20**, 6 (1968)
8. I. Appelbaum, B. Huang, D.J. Monsma, Nature **447**, 295 (2007)
9. S.P. Dash, S. Sharma, R.S. Patel, M.P. de Jong, R. Jansen, Nature **462**, 491 (2009)
10. B.T. Jonker, G. Kioseoglou, A.T. Hanbicki, C.H. Li, P.E. Thompson, Nat. Phys. **3**, 542 (2007)
11. C.H. Li, G. Kioseoglou, O.M.J. van't Erve, P.E. Thompson, B.T. Jonker, Appl. Phys. Lett. **95**, 172102 (2009)
12. T. Suzuki, T. Sasaki, T. Oikawa, M. Shiraishi, Y. Suzuki, K. Noguchi, Appl. Phys. Express **4**, 023003 (2011)
13. O.M.J. van't Erve, A.T. Hanbicki, M. Holub, C.H. Li, C. Awo-Affouda, P.E. Thompson, B.T. Jonker, Appl. Phys. Lett. **91**, 212109 (2007)
14. C.H. Li, O.M.J. van't Erve, B.T. Jonker, Nat. Commun. **2**, 245 (2011)
15. K.-R. Jeon, B.-C. Min, I.-J. Shin, C.-Y. Park, H.-S. Lee, Y.-H. Jo, S.-C. Shin, Appl. Phys. Lett. **98**, 262102 (2011)
16. R. Jansen, B.C. Min, S.P. Dash, S. Sharma, G. Kioseoglou, A.T. Hanbicki, O.M.J. van't Erve, P.E. Thompson, B.T. Jonker, Phys. Rev. B **82**, 241305 (2010)
17. R. Jansen, B.C. Min, S.P. Dash, Nat. Mater. **9**, 133 (2010)
18. J.C.C. Le Breton, S. Sharma, H. Saito, S. Yuasa, R. Jansen, Nature **475**, 82 (2011)
19. E. Shikoh, K. Ando, K. Kubo, E. Saitoh, T. Shinjo, M. Shiraishi, Phys. Rev. Lett. **110**, 127201 (2013)
20. R. Jansen, Nat. Mater. **11**, 400 (2012)
21. T. Sasaki, T. Oikawa, T. Suzuki, M. Shiraishi, Y. Suzuki, K.K. Tagami, Appl. Phys. Express **2**, 053003 (2009)
22. O.M.J. van't Erve, C. Awo-Affouda, A.T. Hanbicki, C.H. Li, P.E. Thompson, B.T. Jonker, IEEE Trans. Electron Devices **56**, 2343 (2009)
23. J. Panda, S. Chattopadhyay, T.K. Nath, Thin Solid Films **546**, 211 (2013)
24. J.M.D. Coey, M. Venkatesan, J. Appl. Phys. **91**, 8345 (2002)

25. YuS Dedkov, U. Rudiger, G. Guntherodt, *Phys. Rev. B* **65**, 064417 (2002)
26. D.J. Huang et al., *J. Magn. Magn. Mater.* **239**, 261 (2002)
27. V.A.M. Brabers, *Handbook of Magnetic Materials*, vol. 8 (Elsevier, New York, 1995), pp. 189–324
28. A.V. Ramos, T.S. Santos, G.X. Miao, M.J. Guittet, J.B. Moussy, J.S. Moodera, *Phys. Rev. B* **78**, 180402(R) (2008)
29. U. Lüders, A. Barthélémy, M. Bibes, K. Bouzehouane, S. Fusil, E. Jacquet, J.P. Contour, J.F. Bobo, J. Fontcuberta, A. Fert, *Adv. Mater. (Weinheim, Germany)* **18**, 1733 (2006)
30. F.X. Cheng, J.T. Jia, Z.G. Xu, B. Zhou, C.S. Liao, C.H. Yan, L.Y. Chen, H.B. Zhao, *J. Appl. Phys.* **86**, 2727 (1999)
31. Y. Kitamoto, S. Kantake, F. Shirasaki, M. Abe, M. Naoe, *J. Appl. Phys.* **85**, 4708 (1999)
32. P.C. Dorsey, P. Lubitz, D.B. Chrisey, J.S. Horwitz, *J. Appl. Phys.* **79**, 6338 (1996)
33. G. Hu, J.H. Choi, C.B. Eom, V.G. Harris, Y. Suzuki, *Phys. Rev. B* **62**, 779 (2000)
34. Y. Suzuki, R.B. van Dover, E.M. Gyorgy, J.M. Phillips, V. Korenivski, D.J. Werder, C.H. Chen, R.J. Cava, J.J. Krajewski, W.F. Peck, K.B. Do, *Appl. Phys. Lett.* **68**, 714 (1996)
35. Y. Suzuki, G. Hu, R.B. van Dover, R.J. Cava, *J. Magn. Magn. Mater.* **191**, 1 (1999)
36. A. Raghunathan, I.C. Nlebedim, D.C. Jiles, J.E. Snyder, *J. Appl. Phys.* **107**, 09A516 (2010)
37. D. Popovic, A.B. Fowler, S. Washburn, *Phys. Rev. Lett.* **79**, 1543 (1997)
38. R.S. Gaikwad, S.-Y. Chae, R.S. Mane, S.-H. Han, O.-S. Joo, *Int. J. Electrochem.* **2011**, 729141 (2011)
39. S.J. May, B.W. Wessels, *Appl. Phys. Lett.* **88**, 072105 (2006)
40. J. Panda, S.N. Saha, T.K. Nath, *Phys. B* **448**, 184–187 (2014)
41. J. Ventura, J.M. Teixeira, J.P. Araujo, J.B. Sousa, *Phys. Rev. B* **78**, 024403 (2008)
42. G. Chakraborty, S. Chattopadhyay, C.K. Sarkar, C. Pramanik, *J. Appl. Phys.* **101**, 024315 (2007)
43. S.D. Ganichev, E. Ziemann, W. Prettl, I.N. Yassievich, A.A. Istratov, E.R. Weber, *Phys. Rev. B* **61**, 10361 (2000)
44. G. Vincent, A. Chantre, D. Bois, *J. Appl. Phys.* **50**, 5484 (1979)
45. W.R. Buchwald, N.M. Johnson, *J. Appl. Phys.* **64**, 958 (1988)
46. L. Tsybeskov, G.F. Grom, P.M. Fauchet, J.P. McCaffrey, J.-M. Baribeau, G.I. Sproule, D.J. Lockwood, *Appl. Phys. Lett.* **75**, 2265 (1999)
47. A. Ilie, B. Equer, *Phys. Rev. B* **57**, 15349 (1998)
48. P.A. Martin, B.G. Streetman, K. Hess, *J. Appl. Phys.* **52**, 7409 (1981)
49. A. Fert, H. Jaffrés, *Phys. Rev. B* **64**, 184420 (2001)
50. A. Dankert, R.S. Dulal, S.P. Dash, *Sci. Rep.* **3**, 3196 (2013)
51. H.W. Zhao, Y. Chen, G.S. Dong, M. Lu, X.F. Jin, Y.J. Wang, H.R. Zhai, D. Yang, R. Naik, G.L. Dunifer, G.W. Auner, *J. Appl. Phys.* **81**, 5203 (1997)
52. R. Adhikari, A. Sarkar, G.R. Patta, A.K. Das, *Appl. Phys. Lett.* **98**, 183504 (2011)
53. A. Sarkar, R. Adhikari, A.K. Das, *Appl. Phys. Lett.* **100**, 262402 (2012)
54. M. Ziese, U. Kohler, A. Bollero, R. Hohne, P. Esquinazi, *Phys. Rev. B* **71**, 180406 (2005)